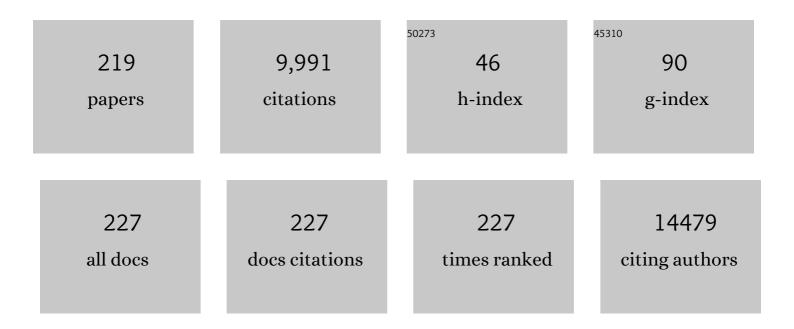
## **Guangming Lu**

List of Publications by Year in descending order

Source: https://exaly.com/author-pdf/9533229/publications.pdf Version: 2024-02-01



#	Article	IF	CITATIONS
1	Evaluation of gray matter reduction in patients with typhoon-related posttraumatic stress disorder using causal network analysis of structural MRI. Psychological Medicine, 2022, 52, 1481-1490.	4.5	5
2	Coronary artery calcification and risk of mortality and adverse outcomes in patients with COVID-19: a Chinese multicenter retrospective cohort study. Chinese Journal of Academic Radiology, 2022, 5, 20-28.	0.6	7
3	Periodic mesoporous organosilica coupled with chlorin e6 and catalase for enhanced photodynamic therapy to treat triple-negative breast cancer. Journal of Colloid and Interface Science, 2022, 610, 634-642.	9.4	8
4	Automated quantitative lesion water uptake in acute stroke is a predictor of malignant cerebral edema. European Radiology, 2022, 32, 2771-2780.	4.5	10
5	Influence of diabetes mellitus on the diagnostic performance of machine learning–based coronary CT angiography–derived fractional flow reserve: a multicenter study. European Radiology, 2022, 32, 3778-3789.	4.5	5
6	One-year outcomes of CCTA alone versus machine learning–based FFRCT for coronary artery disease: a single-center, prospective study. European Radiology, 2022, 32, 5179-5188.	4.5	6
7	Artificial intelligence in imaging of coronary artery disease: current applications and future perspective. Chinese Journal of Academic Radiology, 2022, 5, 10-19.	0.6	0
8	Functional CAD-RADS using FFRCT on therapeutic management and prognosis in patients with coronary artery disease. European Radiology, 2022, 32, 5210-5221.	4.5	7
9	Diagnosis of Cardiac Amyloidosis Using a Radiomics Approach Applied to Late Gadolinium-Enhanced Cardiac Magnetic Resonance Images: A Retrospective, Multicohort, Diagnostic Study. Frontiers in Cardiovascular Medicine, 2022, 9, 818957.	2.4	4
10	Radiomics versus Conventional Assessment to Identify Symptomatic Participants at Carotid Computed Tomography Angiography. Cerebrovascular Diseases, 2022, 51, 647-654.	1.7	6
11	Review of net water uptake in the management of acute ischemic stroke. European Radiology, 2022, 32, 5517-5524.	4.5	10
12	Machine Learning for the Prevalence and Severity of Coronary Artery Calcification in Nondialysis Chronic Kidney Disease Patients. Journal of Thoracic Imaging, 2022, 37, 401-408.	1.5	4
13	Flexible CuS-embedded human serum albumin hollow nanocapsules with peroxidase-like activity for synergistic sonodynamic and photothermal cancer therapy. Nanoscale, 2022, 14, 9702-9714.	5.6	9
14	Gold Nanostar@Polyaniline Theranostic Agent with High Photothermal Conversion Efficiency for Photoacoustic Imaging-Guided Anticancer Phototherapy at a Low Dosage. ACS Applied Materials & Interfaces, 2022, 14, 28570-28580.	8.0	22
15	Altered dynamic parahippocampus functional connectivity in patients with post-traumatic stress disorder. World Journal of Biological Psychiatry, 2021, 22, 236-245.	2.6	17
16	Deformable double-shelled hollow mesoporous organosilica nanocapsules: A multi-interfacial etching strategy. Chinese Chemical Letters, 2021, 32, 1101-1105.	9.0	5
17	Comparison of automated and manual DWI-ASPECTS in acute ischemic stroke: total and region-specific assessment. European Radiology, 2021, 31, 4130-4137.	4.5	18
18	Temporal variability profiling of the default mode across epilepsy subtypes. Epilepsia, 2021, 62, 61-73.	5.1	31

#	Article	IF	CITATIONS
19	The effect of coronary calcification on diagnostic performance of machine learning–based CT-FFR: a Chinese multicenter study. European Radiology, 2021, 31, 1482-1493.	4.5	26
20	Different posterior hippocampus and default mode network modulation in young APOE ε4 carriers: a functional connectome-informed phenotype longitudinal study. Molecular Neurobiology, 2021, 58, 2757-2769.	4.0	7
21	Serial coronary CT angiography–derived fractional flow reserve and plaque progression can predict long-term outcomes of coronary artery disease. European Radiology, 2021, 31, 7110-7120.	4.5	14
22	Machine Learning–Based Prediction of Small Intracranial Aneurysm Rupture Status Using CTA-Derived Hemodynamics: A Multicenter Study. American Journal of Neuroradiology, 2021, 42, 648-654.	2.4	21
23	Detection of renal allograft fibrosis with MRI: arterial spin labeling outperforms reduced field-of-view IVIM. European Radiology, 2021, 31, 6696-6707.	4.5	16
24	Al-based analysis of CT images for rapid triage of COVID-19 patients. Npj Digital Medicine, 2021, 4, 75.	10.9	21
25	Feasibility and prognostic role of machine learning-based FFRCT in patients with stent implantation. European Radiology, 2021, 31, 6592-6604.	4.5	13
26	BCCT: A GUI Toolkit for Brain Structural Covariance Connectivity Analysis on MATLAB. Frontiers in Human Neuroscience, 2021, 15, 641961.	2.0	11
27	Application of lowâ€dose CT to the creation of 3Dâ€printed kidney and perinephric tissue models for laparoscopic nephrectomy. Cancer Medicine, 2021, 10, 3077-3084.	2.8	2
28	A deep-learning pipeline for the diagnosis and discrimination of viral, non-viral and COVID-19 pneumonia from chest X-ray images. Nature Biomedical Engineering, 2021, 5, 509-521.	22.5	106
29	Advanced gastric cancer: CT radiomics prediction and early detection of downstaging with neoadjuvant chemotherapy. European Radiology, 2021, 31, 8765-8774.	4.5	36
30	Distributed Functional Connectome of White Matter in Patients With Functional Dyspepsia. Frontiers in Human Neuroscience, 2021, 15, 589578.	2.0	2
31	Development and validation of a clinically applicable deep learning strategy (HONORS) for pulmonary nodule classification at CT: A retrospective multicentre study. Lung Cancer, 2021, 155, 78-86.	2.0	14
32	ASPECTS-based net water uptake as an imaging biomarker for lesion age in acute ischemic stroke. Journal of Neurology, 2021, 268, 4744-4751.	3.6	12
33	Delayed brain development of Rolandic epilepsy profiled by deep learning–based neuroanatomic imaging. European Radiology, 2021, 31, 9628-9637.	4.5	10
34	Mixed reality models based on low-dose computed tomography technology in nephron-sparing surgery are better than models based on normal-dose computed tomography. Quantitative Imaging in Medicine and Surgery, 2021, 11, 2658-2668.	2.0	5
35	Periodic mesoporous organosilica-coated magnetite nanoparticles combined with lipiodol for transcatheter arterial chemoembolization to inhibit the progression of liver cancer. Journal of Colloid and Interface Science, 2021, 591, 211-220.	9.4	15
36	[18F]PBR146 and [18F]DPA-714 in vivo Imaging of Neuroinflammation in Chronic Hepatic Encephalopathy Rats. Frontiers in Neuroscience, 2021, 15, 678144.	2.8	1

#	Article	IF	CITATIONS
37	GANDA: A deep generative adversarial network conditionally generates intratumoral nanoparticles distribution pixels-to-pixels. Journal of Controlled Release, 2021, 336, 336-343.	9.9	11
38	Deep learning powered coronary CT angiography for detecting obstructive coronary artery disease: The effect of reader experience, calcification and image quality. European Journal of Radiology, 2021, 142, 109835.	2.6	20
39	White Matter Abnormalities in Patients With Typhoon-Related Posttraumatic Stress Disorder. Frontiers in Human Neuroscience, 2021, 15, 665070.	2.0	3
40	Automated ASPECTS for multi-modality CT predict infarct extent and outcome in large-vessel occlusion stroke. European Journal of Radiology, 2021, 143, 109899.	2.6	2
41	Corticoâ€striatoâ€thalamoâ€cerebellar networks of structural covariance underlying different epilepsy syndromes associated with generalized tonic–clonic seizures. Human Brain Mapping, 2021, 42, 1102-1115.	3.6	16
42	Dye-loaded mesoporous polydopamine nanoparticles for multimodal tumor theranostics with enhanced immunogenic cell death. Journal of Nanobiotechnology, 2021, 19, 365.	9.1	27
43	Prognostic Value of Coronary CT Angiography-Derived Fractional Flow Reserve in Non-obstructive Coronary Artery Disease: A Prospective Multicenter Observational Study. Frontiers in Cardiovascular Medicine, 2021, 8, 778010.	2.4	2
44	Postchemotherapy hippocampal functional connectivity patterns in patients with breast cancer: a longitudinal resting state functional MR imaging study. Brain Imaging and Behavior, 2020, 14, 1456-1467.	2.1	25
45	CT FFR for Ischemia-Specific CAD WithÂaÂNew Computational Fluid Dynamics Algorithm. JACC: Cardiovascular Imaging, 2020, 13, 980-990.	5.3	78
46	Similarity and diversity of spontaneous brain activity in functional dyspepsia subtypes. Acta Radiologica, 2020, 61, 927-935.	1.1	7
47	Prognostic implication of CT-FFR based functional SYNTAX score in patients with <i>de novo</i> three-vessel disease. European Heart Journal Cardiovascular Imaging, 2020, , .	1.2	8
48	A clinically applicable deep-learning model for detecting intracranial aneurysm in computed tomography angiography images. Nature Communications, 2020, 11, 6090.	12.8	83
49	Reliability and Reproducibility of the Diameters Method in Rapid Determination of Acute Infarct Volume in Magnetic Resonance Diffusion-Weighted Imaging. Cerebrovascular Diseases, 2020, 49, 575-582.	1.7	4
50	Discrimination between transient and persistent subsolid pulmonary nodules on baseline CT using deep transfer learning. European Radiology, 2020, 30, 6913-6923.	4.5	7
51	Sinogram-Affirmed Iterative Reconstruction Negatively Impacts the Risk Category Based on Agatston Score: A Study Combining Coronary Calcium Score Measurement and Coronary CT Angiography. BioMed Research International, 2020, 2020, 1-10.	1.9	0
52	Altered Functional Integration in the Salience and Default Mode Networks in Euthymic Pediatric Bipolar Disorder. Neural Plasticity, 2020, 2020, 1-9.	2.2	5
53	Impacts of AD-Related ABCA7 and CLU Variants on Default Mode Network Connectivity in Healthy Middle-Age Adults. Frontiers in Molecular Neuroscience, 2020, 13, 145.	2.9	8
54	Orderly Curled Silica Nanosheets with a Small Size and Macromolecular Loading Pores: Synthesis and Delivery of Macromolecules To Eradicate Drug-Resistant Cancer. ACS Applied Materials & Interfaces, 2020, 12, 57810-57820.	8.0	14

#	Article	IF	CITATIONS
55	BSA-Stabilized Mesoporous Organosilica Nanoparticles Reversed Chemotherapy Resistance of Anaplastic Thyroid Cancer by Increasing Drug Uptake and Reducing Cellular Efflux. Frontiers in Molecular Biosciences, 2020, 7, 610084.	3.5	9
56	Risk factors for adverse clinical outcomes with COVID-19 in China: a multicenter, retrospective, observational study. Theranostics, 2020, 10, 6372-6383.	10.0	117
57	Impacts of FKBP5 variants on large-scale brain network connectivity in healthy adults. Journal of Affective Disorders, 2020, 273, 32-40.	4.1	1
58	Impact of machine learning–based coronary computed tomography angiography fractional flow reserve on treatment decisions and clinical outcomes in patients with suspected coronary artery disease. European Radiology, 2020, 30, 5841-5851.	4.5	25
59	Social support modulates the association between PTSD diagnosis and medial frontal volume in Chinese adults who lost their only child. Neurobiology of Stress, 2020, 13, 100227.	4.0	11
60	The clinical application value of mixedâ€realityâ€assisted surgical navigation for laparoscopic nephrectomy. Cancer Medicine, 2020, 9, 5480-5489.	2.8	23
61	Facile synthesis of biodegradable flower-like hydroxyapatite for drug and gene delivery. Journal of Colloid and Interface Science, 2020, 570, 402-410.	9.4	30
62	FKBP5 haplotypes and PTSD modulate the resting-state brain activity in Han Chinese adults who lost their only child. Translational Psychiatry, 2020, 10, 91.	4.8	8
63	Coronavirus Disease 2019 (COVID-19). Journal of Thoracic Imaging, 2020, 35, 234-238.	1.5	3
64	Soft Mesoporous Organosilica Nanoplatforms Improve Blood Circulation, Tumor Accumulation/Penetration, and Photodynamic Efficacy. Nano-Micro Letters, 2020, 12, 137.	27.0	18
65	A deep learning approach to characterize 2019 coronavirus disease (COVID-19) pneumonia in chest CT images. European Radiology, 2020, 30, 6517-6527.	4.5	152
66	Coronavirus Disease 2019 (COVID-19): A Perspective from China. Radiology, 2020, 296, E15-E25.	7.3	1,334
67	Decreased functional connectivity of hippocampal subregions and methylation of the NR3C1 gene in Han Chinese adults who lost their only child. Psychological Medicine, 2020, , 1-10.	4.5	6
68	Enhancing selective photosensitizer accumulation and oxygen supply for high-efficacy photodynamic therapy toward glioma by 5-aminolevulinic acid loaded nanoplatform. Journal of Colloid and Interface Science, 2020, 565, 483-493.	9.4	34
69	The influence of image quality on diagnostic performance of a machine learning–based fractional flow reserve derived from coronary CT angiography. European Radiology, 2020, 30, 2525-2534.	4.5	22
70	Virus-mimicking mesoporous organosilica nanocapsules with soft framework and rough surface for enhanced cellular uptake and tumor penetration. Biomaterials Science, 2020, 8, 2227-2233.	5.4	19
71	Development and validation of machine learning prediction model based on computed tomography angiography–derived hemodynamics for rupture status of intracranial aneurysms: a Chinese multicenter study. European Radiology, 2020, 30, 5170-5182.	4.5	27
72	A bi-adjuvant nanovaccine that potentiates immunogenicity of neoantigen for combination immunotherapy of colorectal cancer. Science Advances, 2020, 6, eaaw6071.	10.3	152

#	Article	IF	CITATIONS
73	Gut dysbiosis-influence on amygdala-based functional activity in patients with end stage renal disease: a preliminary study. Brain Imaging and Behavior, 2020, 14, 2731-2744.	2.1	13
74	Artificial Intelligence in the Management of Intracranial Aneurysms: Current Status and Future Perspectives. American Journal of Neuroradiology, 2020, 41, 373-379.	2.4	54
75	Effects of COMT rs4680 and BDNF rs6265 polymorphisms on brain degree centrality in Han Chinese adults who lost their only child. Translational Psychiatry, 2020, 10, 46.	4.8	12
76	Macroscale and microcircuit dissociation of focal and generalized human epilepsies. Communications Biology, 2020, 3, 244.	4.4	34
77	Coronary Computed Tomography Angiography-Derived Fractional Flow Reserve in Patients with Anomalous Origin of the Right Coronary Artery from the Left Coronary Sinus. Korean Journal of Radiology, 2020, 21, 192.	3.4	19
78	Infection Control and Management Strategy for COVID-19 in the Radiology Department: Focusing on Experiences from China. Korean Journal of Radiology, 2020, 21, 851.	3.4	12
79	Current Status of Etiology, Epidemiology, Clinical Manifestations and Imagings for COVID-19. Korean Journal of Radiology, 2020, 21, 1138.	3.4	7
80	Tube Voltage, DNA Double-Strand Breaks, and Image Quality in Coronary CT Angiography. Korean Journal of Radiology, 2020, 21, 967.	3.4	3
81	Cardiovascular magnetic resonance imaging for amyloidosis: The state-of-the-art. Trends in Cardiovascular Medicine, 2019, 29, 83-94.	4.9	16
82	Uric Acid Has Different Effects on Spontaneous Brain Activities of Males and Females: A Cross-Sectional Resting-State Functional MR Imaging Study. Frontiers in Neuroscience, 2019, 13, 763.	2.8	12
83	Application value of dual-energy computed tomography spectrum curve combined with clinical risk factors in predicting adherent perinephric fat. Quantitative Imaging in Medicine and Surgery, 2019, 9, 1421-1428.	2.0	4
84	Size effect of mesoporous organosilica nanoparticles on tumor penetration and accumulation. Biomaterials Science, 2019, 7, 4790-4799.	5.4	27
85	Diagnostic Performance of Machine Learning Based CT-FFR in Detecting Ischemia in Myocardial Bridging and Concomitant Proximal Atherosclerotic Disease. Canadian Journal of Cardiology, 2019, 35, 1523-1533.	1.7	15
86	Gadolinium-Doped Hydroxyapatite Nanorods as T1 Contrast Agents and Drug Carriers for Breast Cancer Therapy. ACS Applied Nano Materials, 2019, 2, 1194-1201.	5.0	30
87	The effect of prophylactic oral vitamin C use on DNA double-strand breaks after abdominal contrast-enhanced CT: A preliminary study. European Journal of Radiology, 2019, 117, 69-74.	2.6	2
88	Diagnostic performance of fractional flow reserve derived from coronary CT angiography for detection of lesion-specific ischemia: A multi-center study and meta-analysis. European Journal of Radiology, 2019, 116, 90-97.	2.6	41
89	Soft mesoporous organosilica nanorods with gold plasmonic core for significantly enhanced cellular uptake. Journal of Colloid and Interface Science, 2019, 550, 81-89.	9.4	7
90	Generic synthesis of small-sized hollow mesoporous organosilica nanoparticles for oxygen-independent X-ray-activated synergistic therapy. Nature Communications, 2019, 10, 1241.	12.8	112

#	Article	IF	CITATIONS
91	Deteriorated functional and structural brain networks and normally appearing functional–structural coupling in diabetic kidney disease: a graph theory-based magnetic resonance imaging study. European Radiology, 2019, 29, 5577-5589.	4.5	20
92	Coronary CT angiography radiation dose trends: A 10-year analysis to develop institutional diagnostic reference levels. European Journal of Radiology, 2019, 113, 140-147.	2.6	10
93	JQ1-Loaded Polydopamine Nanoplatform Inhibits c-MYC/Programmed Cell Death Ligand 1 to Enhance Photothermal Therapy for Triple-Negative Breast Cancer. ACS Applied Materials & Interfaces, 2019, 11, 46626-46636.	8.0	69
94	Establishment of a novel system for the preoperative prediction of adherent perinephric fat (APF) occurrence based on a multi-mode and multi-parameter analysis of dual-energy CT. Translational Andrology and Urology, 2019, 8, 421-431.	1.4	7
95	The gut microbiota-inflammation-brain axis in end-stage renal disease: perspectives from default mode network. Theranostics, 2019, 9, 8171-8181.	10.0	34
96	The effect of abdominal contrast-enhanced CT on DNA double-strand breaks in peripheral blood lymphocytes: an in vitro and in vivo study. Acta Radiologica, 2019, 60, 687-693.	1.1	7
97	Aberrant Resting-State Functional Connectivity in the Default Mode Network in Pediatric Bipolar Disorder Patients with and without Psychotic Symptoms. Neuroscience Bulletin, 2019, 35, 581-590.	2.9	34
98	Disturbed effective connectivity patterns in an intrinsic triple network model are associated with posttraumatic stress disorder. Neurological Sciences, 2019, 40, 339-349.	1.9	19
99	Computer-assisted detection of acute pulmonary embolism at CT pulmonary angiography in children and young adults: a diagnostic performance analysis. Acta Radiologica, 2019, 60, 1011-1019.	1.1	1
100	Altered resting-state dorsal anterior cingulate cortex functional connectivity in patients with post-traumatic stress disorder. Australian and New Zealand Journal of Psychiatry, 2019, 53, 68-79.	2.3	26
101	Fractional flow reserve derived from CCTA may have a prognostic role in myocardial bridging. European Radiology, 2019, 29, 3017-3026.	4.5	19
102	Sensitive, Real-Time, and In-Vivo Oxygen Monitoring for Photodynamic Therapy by Multifunctional Mesoporous Nanosensors. ACS Applied Materials & Interfaces, 2019, 11, 187-194.	8.0	28
103	Smart Bacterial Magnetic Nanoparticles for Tumor-Targeting Magnetic Resonance Imaging of HER2-Positive Breast Cancers. ACS Applied Materials & Interfaces, 2019, 11, 3654-3665.	8.0	32
104	Mesoporous Organosilica Hollow Nanoparticles: Synthesis and Applications. Advanced Materials, 2019, 31, e1707612.	21.0	179
105	Oxygenâ€Evolving Mesoporous Organosilica Coated Prussian Blue Nanoplatform for Highly Efficient Photodynamic Therapy of Tumors. Advanced Science, 2018, 5, 1700847.	11.2	111
106	High and low molecular weight hyaluronic acid-coated gold nanobipyramids for photothermal therapy. RSC Advances, 2018, 8, 9023-9030.	3.6	25
107	Non-contrast-enhanced magnetic resonance angiography: a reliable clinical tool for evaluating transplant renal artery stenosis. European Radiology, 2018, 28, 4195-4204.	4.5	21
108	Comparison of the effect of radiation exposure from dual-energy CT versus single-energy CT on double-strand breaks at CT pulmonary angiography. European Journal of Radiology, 2018, 101, 92-96.	2.6	9

#	Article	IF	CITATIONS
109	Biodegradable Hollow Mesoporous Organosilica Nanotheranostics for Mild Hyperthermia-Induced Bubble-Enhanced Oxygen-Sensitized Radiotherapy. ACS Nano, 2018, 12, 1580-1591.	14.6	172
110	Adjuvant Photothermal Therapy Inhibits Local Recurrences after Breast-Conserving Surgery with Little Skin Damage. ACS Nano, 2018, 12, 662-670.	14.6	69
111	Deformable Hollow Periodic Mesoporous Organosilica Nanocapsules for Significantly Improved Cellular Uptake. Journal of the American Chemical Society, 2018, 140, 1385-1393.	13.7	168
112	Anti-EGFR Peptide-Conjugated Triangular Gold Nanoplates for Computed Tomography/Photoacoustic Imaging-Guided Photothermal Therapy of Non-Small Cell Lung Cancer. ACS Applied Materials & Interfaces, 2018, 10, 16992-17003.	8.0	60
113	Different Hippocampus Functional Connectivity Patterns in Healthy Young Adults with Mutations of APP/Presenilin-1/2 and APOEε4. Molecular Neurobiology, 2018, 55, 3439-3450.	4.0	21
114	Cisplatin and doxorubicin high-loaded nanodrug based on biocompatible thioether- and ethane-bridged hollow mesoporous organosilica nanoparticles. Journal of Colloid and Interface Science, 2018, 513, 214-221.	9.4	28
115	Ag-HPBs by a coating-etching strategy and their derived injectable implants for enhanced tumor photothermal treatment. Journal of Colloid and Interface Science, 2018, 512, 439-445.	9.4	8
116	Acute kidney injury in patients with nephrotic syndrome undergoing contrast-enhanced CT for suspected venous thromboembolism: a propensity score-matched retrospective cohort study. European Radiology, 2018, 28, 1585-1593.	4.5	15
117	Aberrances of Cortex Excitability and Connectivity Underlying Motor Deficit in Acute Stroke. Neural Plasticity, 2018, 2018, 1-10.	2.2	17
118	Flexible MoS <sub>2</sub> â€Embedded Human Serum Albumin Hollow Nanocapsules with Long Circulation Times and High Targeting Ability for Efficient Tumor Ablation. Advanced Functional Materials, 2018, 28, 1804081.	14.9	35
119	Photosensitizer-loaded biomimetic platform for multimodal imaging-guided synergistic phototherapy. RSC Advances, 2018, 8, 32200-32210.	3.6	5
120	Neuroinflammation in acute hepatic encephalopathy rats: imaging and therapeutic effectiveness evaluation using 11C-PK11195 and 18F-DPA-714 micro-positron emission tomography. Metabolic Brain Disease, 2018, 33, 1733-1742.	2.9	7
121	Dynamic Network Analysis Reveals Altered Temporal Variability in Brain Regions after Stroke: A Longitudinal Resting-State fMRI Study. Neural Plasticity, 2018, 2018, 1-10.	2.2	26
122	Multifunctional Yolk–Shell Mesoporous Silica Obtained via Selectively Etching the Shell: A Therapeutic Nanoplatform for Cancer Therapy. ACS Applied Materials & Interfaces, 2018, 10, 24440-24449.	8.0	13
123	Typhoon-Related Post-Traumatic Stress Disorder and Trauma Might Lead to Functional Integration Abnormalities in Intra- and Inter-Resting State Networks: a Resting-State Fmri Independent Component Analysis. Cellular Physiology and Biochemistry, 2018, 48, 99-110.	1.6	23
124	Functional Evaluation of Transplanted Kidneys with Reduced Field-of-View Diffusion-Weighted Imaging at 3T. Korean Journal of Radiology, 2018, 19, 201.	3.4	16
125	Altered Amygdala Resting-State Functional Connectivity in Maintenance Hemodialysis End-Stage Renal Disease Patients with Depressive Mood. Molecular Neurobiology, 2017, 54, 2223-2233.	4.0	29
126	Lower functional connectivity of default mode network in cognitively normal young adults with mutation of APP, presenilins and APOE $\hat{l}\mu 4.$ Brain Imaging and Behavior, 2017, 11, 818-828.	2.1	16

#	Article	IF	CITATIONS
127	pH-Dependent Transmembrane Activity of Peptide-Functionalized Gold Nanostars for Computed Tomography/Photoacoustic Imaging and Photothermal Therapy. ACS Applied Materials & Interfaces, 2017, 9, 2114-2122.	8.0	67
128	Cerebral CT angiography with iterative reconstruction at 70 kVp and 30 mL iodinated contrast agent: Initial experience. European Journal of Radiology, 2017, 88, 102-108.	2.6	7
129	Tri-stimuli-responsive biodegradable theranostics for mild hyperthermia enhanced chemotherapy. Biomaterials, 2017, 126, 39-48.	11.4	135
130	Periodic Mesoporous Organosilica Coated Prussian Blue for MR/PA Dualâ€Modal Imagingâ€Guided Photothermalâ€Chemotherapy of Triple Negative Breast Cancer. Advanced Science, 2017, 4, 1600356.	11.2	60
131	Severity-specific alterations in CBF, OEF and CMRO2 in cirrhotic patients with hepatic encephalopathy. European Radiology, 2017, 27, 4699-4709.	4.5	19
132	Radiology research in mainland China in the past 10 years: a survey of original articles published in Radiology and European Radiology. European Radiology, 2017, 27, 4379-4382.	4.5	3
133	Prospectively ECG-triggered high-pitch coronary CT angiography at 70 kVp with 30 mL contrast agent: An intraindividual comparison with sequential scanning at 120 kVp with 60 mL contrast agent. European Journal of Radiology, 2017, 90, 97-105.	2.6	21
134	Digital subtraction CT angiography for the detection of posterior inferior cerebellar artery aneurysms: comparison with digital subtraction angiography. European Radiology, 2017, 27, 3744-3751.	4.5	2
135	T 1-Weighted MR/CT dual-modality imaging-guided photothermal therapy using gadolinium-functionalized triangular gold nanoprism. RSC Advances, 2017, 7, 15702-15708.	3.6	8
136	Gold nanorod embedded large-pore mesoporous organosilica nanospheres for gene and photothermal cooperative therapy of triple negative breast cancer. Nanoscale, 2017, 9, 1466-1474.	5.6	39
137	Diabetes Mellitus is Associated with More Severe Brain Spontaneous Activity Impairment and Gray Matter Loss in Patients with Cirrhosis. Scientific Reports, 2017, 7, 7775.	3.3	9
138	Altered spontaneous brain activity pattern in cognitively normal young adults carrying mutations of APP, presenilin-1/2 and APOE Îμ4. European Journal of Radiology, 2017, 95, 18-23.	2.6	3
139	Tumor Acidic Microenvironment Targeted Drug Delivery Based on pHLIP-Modified Mesoporous Organosilica Nanoparticles. ACS Applied Materials & Interfaces, 2017, 9, 30543-30552.	8.0	54
140	Small Intracranial Aneurysms: Diagnostic Accuracy of CT Angiography. Radiology, 2017, 285, 941-952.	7.3	52
141	Radiation Optimized Dual-source Dual-energy Computed Tomography Pulmonary Angiography. Academic Radiology, 2017, 24, 13-21.	2.5	6
142	Disrupted functional connectivity density in irritable bowel syndrome patients. Brain Imaging and Behavior, 2017, 11, 1812-1822.	2.1	36
143	Detection of pulmonary fat embolism with dual-energy CT: an experimental study in rabbits. European Radiology, 2017, 27, 1377-1385.	4.5	3
144	Decreased Coupling Between Functional Connectivity Density and Amplitude of Low Frequency Fluctuation in Non-Neuropsychiatric Systemic Lupus Erythematosus: a Resting-Stage Functional MRI Study. Molecular Neurobiology, 2017, 54, 5225-5235.	4.0	29

#	Article	IF	CITATIONS
145	Hippocampus-associated causal network of structural covariance measuring structural damage progression in temporal lobe epilepsy. Human Brain Mapping, 2017, 38, 753-766.	3.6	61
146	Dynamic functional network connectivity in idiopathic generalized epilepsy with generalized tonic-clonic seizure. Human Brain Mapping, 2017, 38, 957-973.	3.6	275
147	Post-traumatic stress influences local and remote functional connectivity: a resting-state functional magnetic resonance imaging study. Brain Imaging and Behavior, 2017, 11, 1316-1325.	2.1	13
148	Multiparametric functional magnetic resonance imaging for evaluation of hepatic warm ischemia-reperfusion injury in a rabbit model. BMC Gastroenterology, 2017, 17, 161.	2.0	7
149	Altered amygdala and hippocampus effective connectivity in mild cognitive impairment patients with depression: a resting-state functional MR imaging study with granger causality analysis. Oncotarget, 2017, 8, 25021-25031.	1.8	35
150	Early Inflammatory Response following Traumatic Brain Injury in Rabbits Using USPIO- and Gd-Enhanced MRI. BioMed Research International, 2016, 2016, 1-8.	1.9	3
151	18F-DPA-714 PET Imaging for Detecting Neuroinflammation in Rats with Chronic Hepatic Encephalopathy. Theranostics, 2016, 6, 1220-1231.	10.0	14
152	More Severe Extratemporal Damages in Mesial Temporal Lobe Epilepsy With Hippocampal Sclerosis Than That With Other Lesions. Medicine (United States), 2016, 95, e3020.	1.0	19
153	Facile Synthesis of Yolk-Shell-Structured Triple-Hybridized Periodic Mesoporous Organosilica Nanoparticles for Biomedicine. Small, 2016, 12, 3550-3558.	10.0	73
154	Single Phase Dual-energy CT Angiography: One-stop-shop Tool for Evaluating Aneurysmal Subarachnoid Hemorrhage. Scientific Reports, 2016, 6, 26704.	3.3	5
155	Anemia rather than hypertension contributes to cerebral hyperperfusion in young adults undergoing hemodialysis: A phase contrast MRI study. Scientific Reports, 2016, 6, 22346.	3.3	26
156	Aberrant long-range functional connectivity density in generalized tonic-clonic seizures. Medicine (United States), 2016, 95, e3893.	1.0	18
157	Functional Connectome before and following Temporal Lobectomy in Mesial Temporal Lobe Epilepsy. Scientific Reports, 2016, 6, 23153.	3.3	38
158	Image quality, radiation dose and diagnostic accuracy of 70 kVp whole brain volumetric CT perfusion imaging: a preliminary study. European Radiology, 2016, 26, 4184-4193.	4.5	11
159	A Multifunctional PB@mSiO <sub>2</sub> –PEG/DOX Nanoplatform for Combined Photothermal–Chemotherapy of Tumor. ACS Applied Materials & Interfaces, 2016, 8, 17038-17046.	8.0	69
160	Cerebral CTA with Low Tube Voltage and Low Contrast Material Volume for Detection of Intracranial Aneurysms. American Journal of Neuroradiology, 2016, 37, 1774-1780.	2.4	11
161	Resting-state functional MR imaging shed insights into the brain of diabetes. Metabolic Brain Disease, 2016, 31, 993-1002.	2.9	16
162	Selectively Sensitizing Malignant Cells to Photothermal Therapy Using a CD44-Targeting Heat Shock Protein 72 Depletion Nanosystem. ACS Nano, 2016, 10, 8578-8590.	14.6	141

#		Article	IF	CITATIONS
16	3	Synergistic Chemo–Photothermal Therapy of Breast Cancer by Mesenchymal Stem Cell-Encapsulated Yolk–Shell GNR@HPMO-PTX Nanospheres. ACS Applied Materials & Interfaces, 2016, 8, 17927-17935.	8.0	63
16	•4	Neural, electrophysiological and anatomical basis of brain-network variability and its characteristic changes in mental disorders. Brain, 2016, 139, 2307-2321.	7.6	292
16	5	Abnormal Intrinsic Brain Activity Patterns in Patients with End-Stage Renal Disease Undergoing Peritoneal Dialysis: A Resting-State Functional MR Imaging Study. Radiology, 2016, 278, 181-189.	7.3	52
16	6	Chronic thromboembolic pulmonary hypertension: Comparison of dual-energy computed tomography and single photon emission computed tomography in canines. European Journal of Radiology, 2016, 85, 498-506.	2.6	11
16	7	Smart Cancer Cell Targeting Imaging and Drug Delivery System by Systematically Engineering Periodic Mesoporous Organosilica Nanoparticles. ACS Applied Materials & Interfaces, 2016, 8, 2985-2993.	8.0	80
16	8	Abnormal Amygdala Resting-State Functional Connectivity in Irritable Bowel Syndrome. American Journal of Neuroradiology, 2016, 37, 1139-1145.	2.4	40
16	9	Intrinsic brain abnormalities in irritable bowel syndrome and effect of anxiety and depression. Brain Imaging and Behavior, 2016, 10, 1127-1134.	2.1	55
17	0	Topological Reorganization of the Default Mode Network in Irritable Bowel Syndrome. Molecular Neurobiology, 2016, 53, 6585-6593.	4.0	41
17	1	Prospectively ECG-triggered high-pitch 80 kVp coronary computed tomography angiography with 30 mL of 270 mg I/mL contrast material and iterative reconstruction. Acta Radiologica, 2016, 57, 287-294.	1.1	6
17	2	Whole-brain CT perfusion combined with CT angiography for ischemic complications following microsurgical clipping and endovascular coiling of ruptured intracranial aneurysms. Journal of Clinical Neuroscience, 2016, 26, 50-56.	1.5	3
17	3	Contrast-induced nephropathy in CT: incidence, risk factors and strategies for prevention. European Radiology, 2016, 26, 3310-3318.	4.5	61
17	4	Image quality, radiation dose, and diagnostic accuracy of prospectively ECG-triggered high-pitch coronary CT angiography at 70ÂkVp in a clinical setting: comparison with invasive coronary angiography. European Radiology, 2016, 26, 797-806.	4.5	49
17	5	Elevated global cerebral blood flow, oxygen extraction fraction and unchanged metabolic rate of oxygen in young adults with end-stage renal disease: an MRI study. European Radiology, 2016, 26, 1732-1741.	4.5	20
17	6	Brain Default Mode Network Changes after Renal Transplantation: A Diffusion-Tensor Imaging and Resting-State Functional MR Imaging Study. Radiology, 2016, 278, 485-495.	7.3	35
17	7	Role of local and distant functional connectivity density in the development of minimal hepatic encephalopathy. Scientific Reports, 2015, 5, 13720.	3.3	16
17	8	Carbogen gas-challenge blood oxygen level-dependent magnetic resonance imaging in hepatocellular carcinoma: Initial results. Oncology Letters, 2015, 10, 2009-2014.	1.8	12
17	9	Effects of transforming growth factor β-1 infected human bone marrow mesenchymal stem cells on high- and low-metastatic potential hepatocellular carcinoma. European Journal of Medical Research, 2015, 20, 56.	2.2	13
18	0	Multimodality MRI Findings in Patients with End-Stage Renal Disease. BioMed Research International, 2015, 2015, 1-12.	1.9	16

#	Article	IF	CITATIONS
181	A Facile Multi-interface Transformation Approach to Monodisperse Multiple-Shelled Periodic Mesoporous Organosilica Hollow Spheres. Journal of the American Chemical Society, 2015, 137, 7935-7944.	13.7	238
182	Image quality and radiation dose of lower extremity CT angiography at 70 kVp on an integrated circuit detector dual-source computed tomography. Acta Radiologica, 2015, 56, 659-665.	1.1	17
183	Seventy–Peak Kilovoltage High-Pitch Thoracic Aortic CT Angiography without ECG Gating. Academic Radiology, 2015, 22, 890-897.	2.5	19
184	Hemodynamic alterations in unilateral chronic middle cerebral artery stenosis patients and the effect of percutaneous transluminal angioplasty and stenting: a perfusion-computed tomography study. Acta Radiologica, 2015, 56, 754-760.	1.1	14
185	Reversibly Extracellular pH Controlled Cellular Uptake and Photothermal Therapy by PEGylated Mixed-Charge Gold Nanostars. Small, 2015, 11, 1801-1810.	10.0	74
186	Gold nanostars functionalized with amine-terminated PEG for X-ray/CT imaging and photothermal therapy. Journal of Materials Chemistry B, 2015, 3, 4330-4337.	5.8	42
187	Radiation dose and image quality of 70 kVp cerebral CT angiography with optimized sinogram-affirmed iterative reconstruction: comparison with 120 kVp cerebral CT angiography. European Radiology, 2015, 25, 1453-1463.	4.5	37
188	70-kVp High-pitch Computed Tomography Pulmonary Angiography with 40 mL Contrast Agent. Academic Radiology, 2015, 22, 1562-1570.	2.5	29
189	The brain following transjugular intrahepatic portosystemic shunt: the perspective from neuroimaging. Metabolic Brain Disease, 2015, 30, 1331-1341.	2.9	0
190	Quantitative measurements of brain iron deposition in cirrhotic patients using susceptibility mapping. Acta Radiologica, 2015, 56, 339-346.	1.1	18
191	Altered Modular Organization of Functional Connectivity Networks in Cirrhotic Patients without Overt Hepatic Encephalopathy. BioMed Research International, 2014, 2014, 1-11.	1.9	10
192	High-pitch computed tomography pulmonary angiography with iterative reconstruction at 80 kVp and 20 mL contrast agent volume. European Radiology, 2014, 24, 3260-3268.	4.5	71
193	High-Pitch Coronary CT Angiography at 70 kVp With Low Contrast Medium Volume. Medicine (United) Tj ETQq1 🕻	1 0.78431 1.0	4.rgBT /Ove
194	Novel CT-guided coil localization of peripheral pulmonary nodules prior to video-assisted thoracoscopic surgery: a pilot study. Acta Radiologica, 2014, 55, 699-706.	1.1	42
195	Facile Synthesis of Yolk–Shell Structured Inorganic–Organic Hybrid Spheres with Ordered Radial Mesochannels. Advanced Materials, 2014, 26, 3741-3747.	21.0	181
196	In Vivo Volumetric Photoacoustic Molecular Angiography and Therapeutic Monitoring with Targeted Plasmonic Nanostars. Small, 2014, 10, 1585-1593.	10.0	157
197	Prevalence and types of coronary to pulmonary artery fistula in a Chinese population at dual-source CT coronary angiography. Acta Radiologica, 2014, 55, 1031-1039.	1.1	21
198	<i>DynamicBC</i> : A MATLAB Toolbox for Dynamic Brain Connectome Analysis. Brain Connectivity, 2014, 4, 780-790.	1.7	221

#	Article	IF	CITATIONS
199	Disrupted small world networks in patients without overt hepatic encephalopathy: A resting state fMRI study. European Journal of Radiology, 2014, 83, 1890-1899.	2.6	33
200	Yolk–Shell Structured Mesoporous Nanoparticles with Thioether-Bridged Organosilica Frameworks. Chemistry of Materials, 2014, 26, 5980-5987.	6.7	94
201	Alterations of regional homogeneity in pediatric bipolar depression: a resting-state fMRI study. BMC Psychiatry, 2014, 14, 222.	2.6	43
202	Feasibility of prospectively ECG-triggered high-pitch coronary CT angiography with 30ÂmL iodinated contrast agent at 70ÂkVp: initial experience. European Radiology, 2014, 24, 1537-1546.	4.5	58
203	Brain regional homogeneity changes following transjugular intrahepatic portosystemic shunt in cirrhotic patients support cerebral adaptability theory—A resting-state functional MRI study. European Journal of Radiology, 2014, 83, 578-583.	2.6	14
204	Multidetector Computed Tomography of Superior Mesenteric Artery: Anatomy and Pathologies. Canadian Association of Radiologists Journal, 2014, 65, 267-274.	2.0	6
205	Abnormal functional connectivity within the default mode network in patients with HBV-related cirrhosis without hepatic encephalopathy revealed by resting-state functional MRI. Brain Research, 2014, 1576, 73-80.	2.2	18
206	Emphasize the Effect of Methylphenidate on Brain Function in Attention-Deficit/Hyperactivity Disorder Research. JAMA Psychiatry, 2014, 71, 210.	11.0	4
207	Image Quality and Radiation Dose of Lower Extremity CT Angiography Using 70 kVp, High Pitch Acquisition and Sinogram-Affirmed Iterative Reconstruction. PLoS ONE, 2014, 9, e99112.	2.5	30
208	Impaired self-referential processing in mesial temporal lobe epilepsy: A functional MRI study. Neuroscience Letters, 2013, 555, 187-192.	2.1	5
209	Mesoporous Silica Hollow Spheres with Ordered Radial Mesochannels by a Spontaneous Self-Transformation Approach. Chemistry of Materials, 2013, 25, 98-105.	6.7	203
210	Relationship Between Large-Scale Functional and Structural Covariance Networks in Idiopathic Generalized Epilepsy. Brain Connectivity, 2013, 3, 240-254.	1.7	66
211	Single Continuous Wave Laser Induced Photodynamic/Plasmonic Photothermal Therapy Using Photosensitizerâ€Functionalized Gold Nanostars. Advanced Materials, 2013, 25, 3055-3061.	21.0	453
212	Increasing Cellular Uptake of Mesoporous Silica Nanoparticles in Human Embryonic Kidney Cell Line 293T Cells by Using Lipofectamine 2000. Journal of Biomedical Nanotechnology, 2013, 9, 1882-1890.	1.1	22
213	Dual-Energy CT of the Lung. American Journal of Roentgenology, 2012, 199, S40-S53.	2.2	135
214	Impairments of Thalamic Nuclei in Idiopathic Generalized Epilepsy Revealed by a Study Combining Morphological and Functional Connectivity MRI. PLoS ONE, 2012, 7, e39701.	2.5	65
215	Microstructural changes in memory and reticular formation neural pathway after simple concussion. Neural Regeneration Research, 2012, 7, 2206-12.	3.0	1
216	Altered functional–structural coupling of large-scale brain networks in idiopathic generalized epilepsy. Brain, 2011, 134, 2912-2928.	7.6	486

#	Article	IF	CITATIONS
217	Altered resting state networks in epileptic patients with generalized tonic–clonic seizures. Brain Research, 2011, 1374, 134-141.	2.2	98
218	Applications of Gold Nanoparticles in Cancer Imaging and Treatment. , 0, , .		9
219	The correlation study on chest CT features and kidney injury in severe COVID-19 pneumonia from a multicenter cohort study. Chinese Journal of Academic Radiology, 0, , .	0.6	1